Crystals **2011**, *1*, 206-214; doi:10.3390/cryst1030206

OPEN ACCESS

crystals

ISSN 2073-4352

www.mdpi.com/journal/crystals

Article

$Ba_5Cd_2Sb_4O_2$—A New Antimonide Oxide with a Complex Structure

Gregory M. Darone, and Svilen Bobev *

Department of Chemistry and Biochemistry, University of Delaware, Newark, DE 19716, USA

* Author to whom correspondence should be addressed; E-Mail: bobev@udel.edu; Tel.: +1-302-831-8720; Fax: +1-302-831-6335.

Received: 18 August 2011; in revised form: 14 September 2011 / Accepted: 19 September 2011 / Published: 20 September 2011

Abstract: Synthesis and single-crystal X-ray structure determination of the new antimonide oxide, $Ba_5Cd_2Sb_4O_2$ are reported. $Ba_5Cd_2Sb_4O_2$ crystallizes in the monoclinic space group *C2/m* (No. 12) with unit cell parameters: a = 17.247(7) Å, b = 4.9279(18) Å, c = 12.240(5) Å, and β = 132.558(4)°; Z = 2. Its crystal structure can be described as a polyanionic $^{2}_{\infty}[Cd_2Sb_4]^{6-}$ sub-lattice made up of fused $CdSb_4$ tetrahedra, stacked between puckered slabs of oxo-anions, O^{2-}, and Ba^{2+} cations. This structure can also be described as a "double-salt", *i.e.*, a structure composed of fragments from the Zintl phase $Ba_3Cd_2Sb_4$ intercalated by two BaO-like moieties. The topological similarities between the structures of these compounds are discussed.

Keywords: barium; cadmium; antimonide; oxide

1. Introduction

Complex pnictide-oxide structures have been investigated for nearly two decades [1], however they have garnered more interest lately because of the surprising discovery of high temperature superconductivity within their realm [2]. For example, Fe-based arsenic-oxides, such as $SmFeAsO_{\sim 0.85}$, have displayed superconductivity at temperatures as high as 55 K [3]. Over the past seven years, our research group has systematically explored the alkaline-earth metal and rare-earth metal antimonide systems. The resulting new compounds have often been Zintl phases [4-6] with complex crystal and electronic structures, and unusual properties [7-20]. Although oxide research is not our focus, it is sometimes the case that adventurous oxygen molecules find their way into our experiments and

surprise us with an atypical compound, such as the previously reported $Ba_5Cd_2Sb_5O_x$ ($0.5 < x < 0.7$) [17].

In a more recent experiment, serendipitous oxidation during the synthesis of a reaction containing Ba, Cd, and Sb occurred. Upon inspection, several atypical (for an intermetallic compound) crystals were identified among the reaction's main product, $BaCdSb_2$ [21]—these turned out to be crystals of the novel antimonide oxide, $Ba_5Cd_2Sb_4O_2$, which is the subject of this paper.

2. Results and Discussion

$Ba_5Cd_2Sb_4O_2$ crystallizes in the monoclinic space group *C2/m* (No. 12), and its crystal structure contains three unique barium positions, one unique cadmium position, two unique antimony positions, and one unique oxygen position in the asymmetric unit (Tables 1 and 2). The structure is best described as polyanionic $^{2}_{\infty}[Cd_2Sb_4]^{6-}$ layers made up of edge-shared $CdSb_4$ tetrahedra extending along the *b* axis, with O^{2-} anions and Ba^{2+} cations between them (Figure 1). The structure is similar to that of the previously reported Zintl phase $Ba_3Cd_2Sb_4$ (also with space group *C2/m*) [12]. In fact, their lattice parameters are quite similar—a = 17.247(7) Å; b = 4.9279(18) Å; c = 12.240(5) Å; β = 132.558(4)° for the former and a = 17.835(2) Å, b = 4.8675(5) Å, c = 7.6837(7) Å, and β = 112.214(1)° for the latter. Recognizing this relationship and noting the expansion in the *c* axis and β angle, we can consider the $Ba_5Cd_2Sb_4O_2$ structure to be a 1:2 intergrowth of $Ba_3Cd_2Sb_4$ and BaO fragments, *i.e.*, the formula can be broken down as follows:

$$\mathbf{Ba_5Cd_2Sb_4O_2 = Ba_3Cd_2Sb_4 + 2 \times BaO}$$

Table 1. Selected crystal data and structure refinement parameters for $Ba_5Cd_2Sb_4O_2$.

Empirical formula	$Ba_5Cd_2Sb_4O_2$
Formula weight/ g·mol^{-1}	1430.5
Crystal system	Monoclinic
Space group	*C2/m*
Z	2
T / K	200(2)
a/ Å	17.247(7)
b/ Å	4.9279(18)
c/ Å	12.240(5)
β/ °	132.558(4)
V/ Å^3	766.3(5)
ρ_{calc}/ g·cm^{-3}	6.200
μ(Mo-Kα)/ cm^{-1}	222.3
Crystal size/ mm	0.072 × 0.070 × 0.056
Reflections collected	3359
Independent reflections	1147
Goodness-of-fit	1.048
R_1 ($I > 2\sigma_{(I)}$)[a]	0.0241
wR_2 ($I > 2\sigma_{(I)}$)[a]	0.0492
R_1 (all data)[a]	0.0291
wR_2 (all data)[a]	0.0513
Largest peak and hole/ e$^-$·Å^{-3}	1.198; –2.176

[a] $R_1 = \sum||F_o| - |F_c||/\sum|F_o|$, $wR_2 = [\sum[w(F_o^2 - F_c^2)^2]/\sum[w(F_o^2)^2]]^{1/2}$, and $w = 1/[\sigma^2F_o^2 + (0.022\cdot P)^2]$, $P = (F_o^2 + 2F_c^2)/3$.

Table 2. Atomic coordinates and equivalent isotropic displacement parameters (U_{eq}[a]).

Atom	Wyckoff site	*x*	*y*	*z*	U_{eq}/ Å^2
Ba1	4*i*	0.02659(3)	0	0.70308(5)	0.0100(1)
Ba2	4*i*	0.29970(3)	0	0.64996(5)	0.0145(1)
Ba3	2*a*	0	0	0	0.0182(2)
Cd	4*i*	0.26114(4)	0	0.12247(6)	0.0114(1)
Sb1	4*i*	0.36548(3)	0	0.01038(5)	0.0096(1)
Sb2	4*i*	0.39272(4)	0	0.43332(5)	0.0098(1)
O	4*i*	0.1297(4)	0	0.3132(7)	0.0182(1)

[a] U_{eq} is defined as one third of the trace of the orthogonalized U_{ij} tensor.

Figure 1. Perspective view down the *b* axis of the monoclinic crystal structure of $Ba_5Cd_2Sb_4O_2$ with unit cell outlined. Ba atoms are represented with red spheres, Cd atoms with blue spheres, Sb atoms with gold spheres, and O atoms with green spheres.

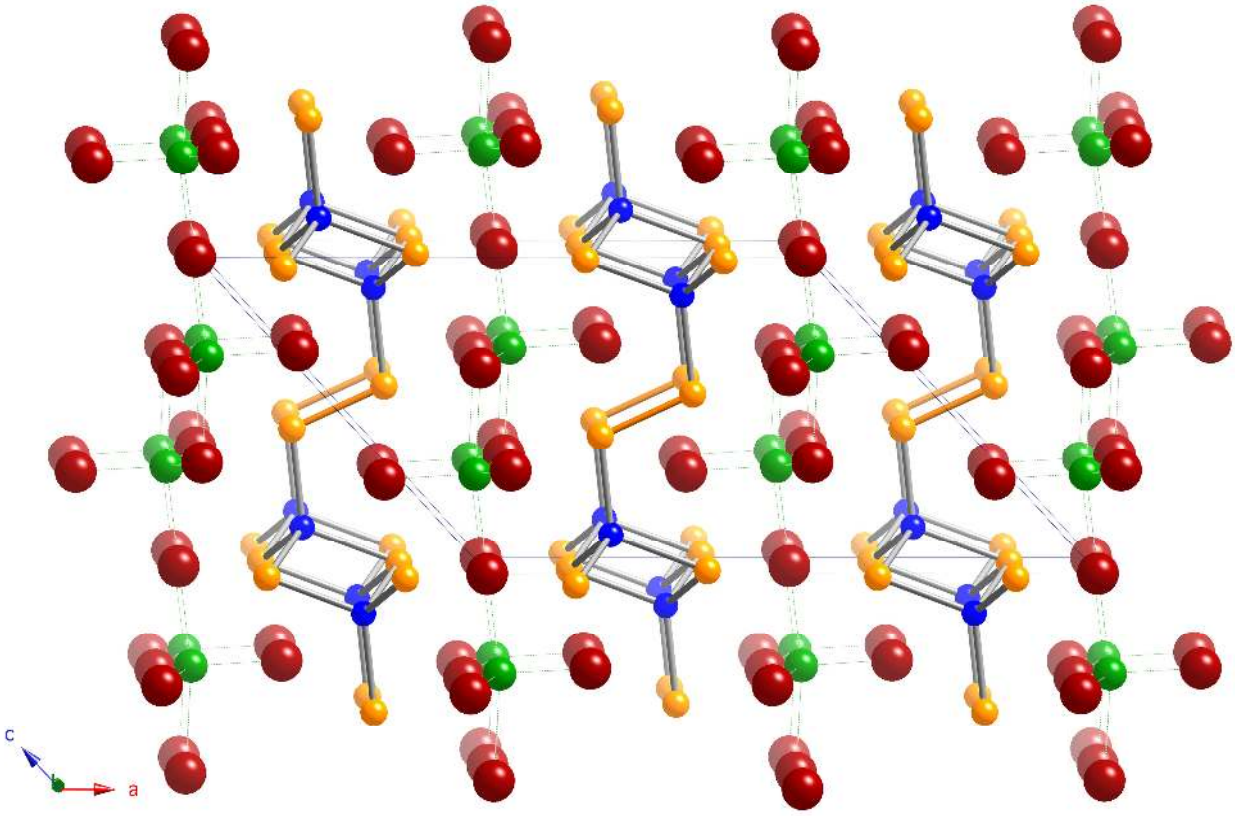

A schematic representation of this idea, also showing how the parent $Ba_3Cd_2Sb_4$ structure distorts to accommodate the O^{2-} anions and the additional Ba^{2+} cations is shown in Figure 2.

Figure 2. (a) Perspective view down the *b* axis of the monoclinic crystal structure of the Zintl phase $Ba_3Cd_2Sb_4$ [12]. (b) Space available for BaO fragments. Notice how the parent $^{2}_{\infty}[Cd_2Sb_4]^{6-}$ layers are stretched and shifted, and the space between the layers is expanded. (c) Crystal structure of $Ba_5Cd_2Sb_4O_2$. Color code is identical to that in Figure 1.

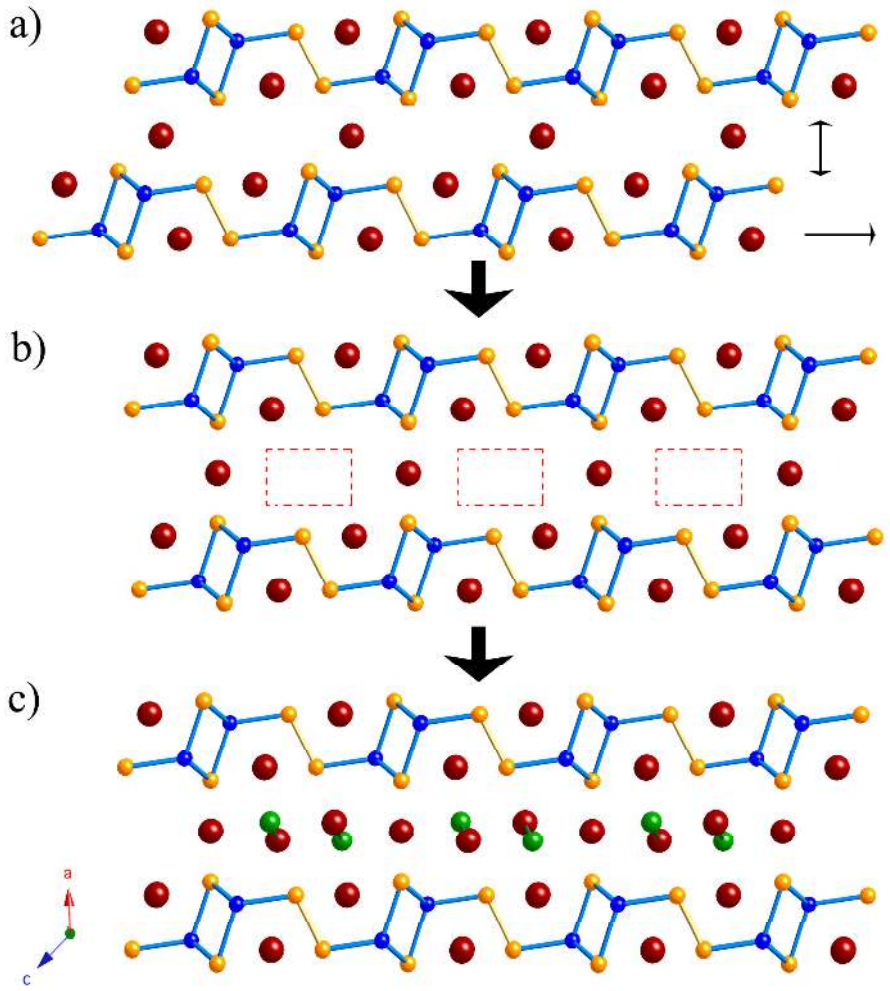

The length of the Cd–Sb bonds in $Ba_5Cd_2Sb_4O_2$ range from 2.8190(13) Å to 2.9463(9) Å, with Sb-Cd-Sb angles varying from 101.76(3)° to 116.52(4)°. These distances and angles are very similar to those reported for $Ba_3Cd_2Sb_4$. More specifically, the length of the Cd–Sb bonds in $Ba_3Cd_2Sb_4$ range from 2.9125(4) Å to 2.9531(5) Å, with Sb-Cd-Sb angles ranging from 101.95(1)° to 113.36(2)°.

Just like in $Ba_3Cd_2Sb_4$, the $CdSb_4$ tetrahedra within the polyanionic $^{2}_{\infty}[Cd_2Sb_4]^{6-}$ layers of $Ba_5Cd_2Sb_4O_2$ are "bridged" through Sb–Sb bonds, which measure 2.8615(16) Å. Compared with $Ba_3Cd_2Sb_4$, where the Sb–Sb bond length is 2.8114(8) Å, one sees a slight elongation, consistent with the idea that the Cd_2Sb_4 layers in the parent structure have been "stretched" in order to accommodate the Ba-O slabs. We also draw attention to the fact that in both $Ba_5Cd_2Sb_4O_2$ and $Ba_3Cd_2Sb_4$, the Sb–Sb distance is shorter than the 2.908 Å distance found in elemental Sb [22], indicating a strong covalent character for that bonding interaction.

The Ba–O fragments do not resemble the actual structure of BaO (NaCl type). The "BaO" layers in $Ba_5Cd_2Sb_4O_2$ are composed of Ba2 and O atom positions (Table 2), and are inserted into the

$Ba_3Cd_2Sb_4$ structure template between the existing Ba1 and Ba3 atom positions. In this case, the neighboring Ba atoms form a distorted, square pyramidal, five-coordinate bonding environment around the O, with the Ba–O bond lengths on the order of 2.565(5) Å to 3.040(6) Å. These distances are comparable to the Ba–O bond lengths of 2.628(6) Å to 2.766(4) Å found in a similar compound, $Ba_5Cd_2Sb_5O_x$ ($0.5 < x < 0.7$) [17]. As seen in Figure 3, the O^{2-} ions in $Ba_5Cd_2Sb_5O_x$ ($0.5 < x < 0.7$) exist in a tetrahedral environment, where the Ba_4O-tetrahedra share corners to form an infinite chain. In $Ba_5Cd_2Sb_4O_2$, however, the O^{2-} ions are found in a five-coordinate environment of Ba^{2+} cations. The shape of such a coordination polyhedron resembles a distorted square pyramid; the latter share edges and corners to form an infinite puckered ribbon.

Figure 3. Coordination environment of the O^{2-} ion in $Ba_5Cd_2Sb_5O_x$ ($0.5 < x < 0.7$) (a), and in $Ba_5Cd_2Sb_4O_2$ (b). Relevant interatomic distances are indicated. Color code is identical to that of Figure 1.

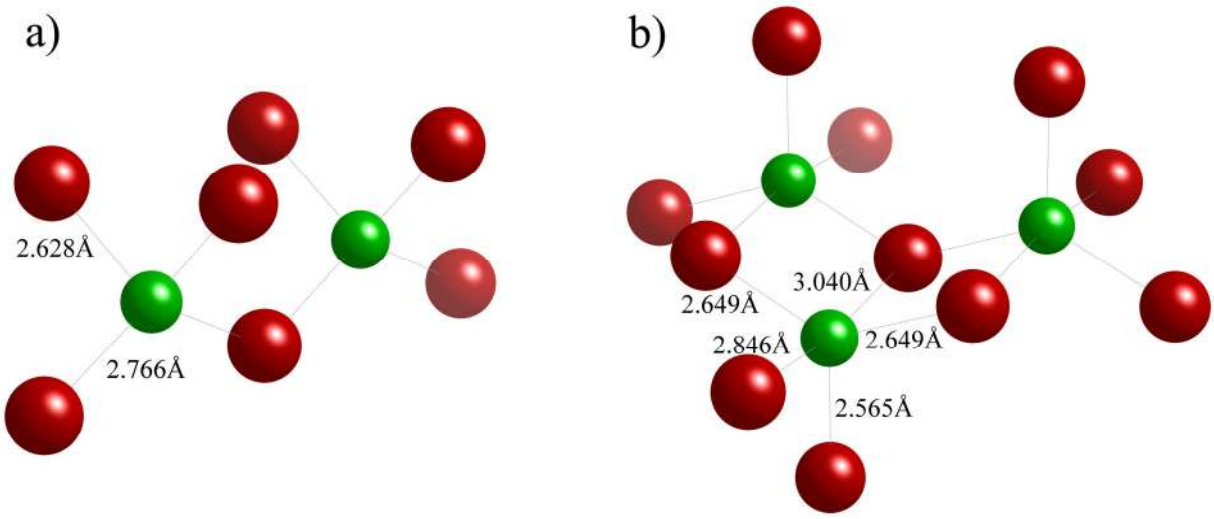

$Ba_5Cd_2Sb_4O_2$ is an electron precise, salt-like compound, where the electron count conforms to the Zintl-Klemm rules [4,5]. In addition to the notion of it being a "double-salt", as described above, the formula can be rationalized as:

$$5 \times [Ba^{2+}] + 2 \times [Cd^{2+}] + 2 \times [Sb^{2-}] + 2 \times [Sb^{3-}] + 2 \times [O^{2-}] = 0$$

where the two different types of antimony atoms are the ones that are connected through a homoatomic Sb–Sb bond, and the ones that are only bound to Cd atoms, respectively. This simplistic structure rationalization is nicely supported by the electronic structure calculations, which show a band gap of about 0.3 eV at the Fermi level, indicative of a closed-shell system. As shown in Figure 4, just below the Fermi level, the main contributors to the DOS are the Sb p bands, admixed with states originated from Cd and Ba orbitals. The oxygen p bands are filled and situated *ca.* 2 eV below the top of the valence band, corroborating the assignment of the oxygen atoms as oxo-anions.

Figure 4. Total and partial density of states plots (DOS) for $Ba_5Cd_2Sb_4O_2$. Contributions from different elements are color-coded. The Fermi level is depicted as a horizontal dotted line as a reference point at zero energy.

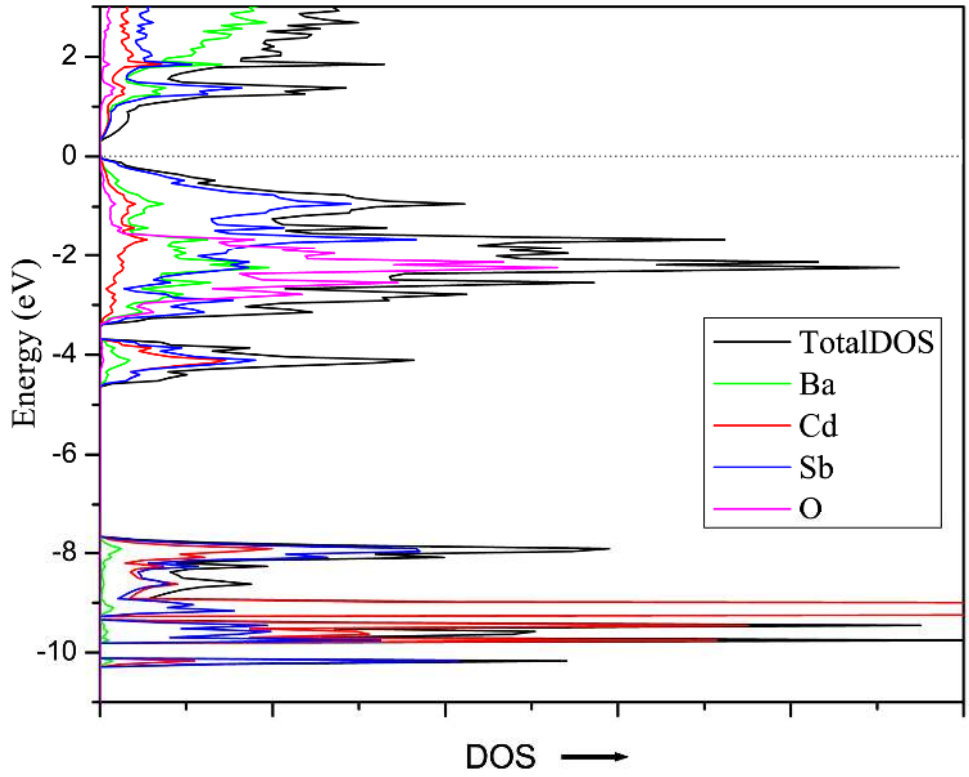

Based on electron counting and DOS calculations, and in an agreement with the dark-colored and brittle habits of the $Ba_5Cd_2Sb_4O_2$ crystals, it is likely that this new antimonide oxide will exhibit semiconducting behavior. Regrettably, resistivity measurements were impeded because of the material's extreme sensitivity to air, and we were unable to experimentally confirm this.

3. Experimental Section

Handling of all materials was performed inside an argon-filled glove-box with oxygen and moisture levels below 0.5 ppm, or under vacuum. Ba, Cd, Sb, and Pb were purchased from Alfa or Aldrich with stated purity greater than 99.9% and were used as received. Single crystals of $Ba_5Cd_2Sb_4O_2$ were synthesized using the metal flux method. Ba, Cd, and Sb were measured in the elemental ratio of 6:4:7 and combined in an alumina crucible with an excess of Pb (ca. 10×, based on molar Ba content) and sealed in an evacuated fused silica jacket. The ampoule was heated in a programmable furnace from 100 °C to 1000 °C at a rate of 100 °C/h, allowed to homogenize at this temperature for 29 h, then cooled to 850 °C at a rate of –1.5 °C/h, and then cooled to 600 °C at a rate of –10 °C/h. At 600 °C, the ampoule was removed from the furnace, inverted, and spun in a centrifuge for 30 seconds to separate the Pb from the crystals. The ampoule was opened inside the argon-filled glove-box for inspection.

From this reaction, the majority phase was identified as $BaCdSb_2$, however several plank-like single crystals of $Ba_5Cd_2Sb_4O_2$ were identified and selected for single-crystal X-ray diffraction. Crystals of $Ba_5Cd_2Sb_4O_2$ removed from the glove-box and exposed to the air and moisture in the laboratory

decomposed and became tarnished, pockmarked, and brittle over 36 h. Because of the air-sensitivity of these crystals, no property measurements were attempted.

Single-crystal X-ray diffraction was performed on a single crystal of $Ba_5Cd_2Sb_4O_2$ selected inside the argon-filled glove-box and placed in Paratone-N oil. This crystal was then quickly removed from the glove-box and cut to suitable dimensions (less than 0.1 mm) under the microscope and placed on the tip of a glass fiber on the goniometer of a Bruker SMART CCD-based diffractometer [23]. The crystal was checked for quality, and full spheres of diffraction data were collected in four batch runs. Although the crystal was air-sensitive, the Paratone-N oil coating the surface of the crystal and the cold stream of nitrogen gas (*ca*. 200(2) K) protected it, and no sign of deterioration during the data collection was observed. SAINTPLUS was used for reduction and integration of the raw data [24]. Semi-empirical absorption correction based on equivalents (*i.e.*, multi-scan) was applied with the SADABS software [25]. The SHELXTL software package was used for structure solution and refinement [26]. Direct methods found the position of all seven unique atoms in the *C2/m* space group. The atomic coordinates were standardized using STRUCTURE TIDY, and anisotropic displacement parameters were included in the final least squares refinements and resulted in a featureless difference Fourier map [27]. Selected details of the data collections and structure refinement parameters are summarized in Table 1. The refined atomic coordinates and equivalent isotropic displacement parameters are given in Table 2.

Additional details of the crystal structure investigations may be obtained from the Fachinformationszentrum Karlsruhe, D-76344 Eggenstein-Leopoldshafen, Germany (Fax: +49-7247-808-666, E-Mail: crysdata@fiz-karlsruhe.de) on quoting the depository numbers CSD-423458.

TB-LMTO-ASA electronic structure calculations for $Ba_5Cd_2Sb_4O_2$ were performed using the LMTO-4.7 package [28]. This program is based on the tight-binding linear muffin-tin orbital (LMTO) method in the local density (LDA) and atomic sphere (ASA) approximations [29-32]. Atomic sphere radii used in the calculations were chosen using an automated procedure, and interstitial spheres were inserted to achieve the space filling automatically [33]. The Fermi level was selected as the energy reference ($\varepsilon_F = 0$ eV).

4. Conclusions

$Ba_5Cd_2Sb_4O_2$ crystallizes in the monoclinic space group *C2/m* and its crystal structure can be derived from that of a similar compound, $Ba_3Cd_2Sb_4$, which has been distorted and augmented. The Cd–Sb, Sb–Sb, and Ba–O bond lengths and Sb-Cd-Sb bond angles agree with those of similar compounds. The frailty of $Ba_5Cd_2Sb_4O_2$ limits its utility to that of a laboratory curiosity, however there are undoubtedly more robust, and more interesting pnictide-oxide compounds waiting to be synthesized.

Acknowledgments

The authors offer sincere thanks for the financial support provided for this research by the University of Delaware and the Undergraduate Research Program.

References

1. Zimmer, B.I.; Jeitschko, W.; Albering, J.H.; Glaum, R.; Reehuis, M. The rare earth transition metal oxides *Ln*FePO, *Ln*RuPO and *Ln*CoPO with ZrCuSiAs type structure. *J. Alloys Compd*. **1995**, *229*, 238-242.
2. Kamihara, Y.; Hiramatsu, H.; Hirano, M.; Kawamura, R.; Yanagi, H.; Kamiya, T.; Hosono, H. Iron-Based Layered Superconductor: LaOFeP. *J. Am. Chem. Soc*. **2006**, *128*, 10012-10013.
3. Ren, Z.-A.; Che, G.-C.; Dong, X.-L.; Yang, J.; Lu, W.; Yi, W.; Shen, X.-L.; Li, Z.-C.; Sun, L.-L.; Zhou, F.; Zhao, Z.-X. Superconductivity and phase diagram in iron-based arsenic-oxides *RE*FeAsO$_{1-\delta}$ (*RE* = rare-earth metal) without fluorine doping. *Europhys. Lett.* **2008**, *83*, 17002.
4. Zintl, E. Intermetallische Verbindungen. *Angew. Chem.* **1939**, *52*, 1-6.
5. Schäfer, H.; Eisenman. B.; Müller, W. Zintl phases—transitions between metallic and ionic bonding. *Angew. Chem. Int. Ed.* **1973**, *12*, 694-712.
6. Kauzlarich, S.M., Ed. *Chemistry, Structure and Bonding of Zintl Phases and Ions*; VCH: Weinheim, Germany, 1996.
7. Bobev, S.; Fritsch, V.; Thompson, J.D.; Sarrao, J.L.; Eck, B.; Dronskowski, R.; Kauzlarich, S.M. Synthesis, structure and properties of the new rare-earth Zintl phase $Yb_{11}GaSb_9$. *J. Solid State Chem.* **2005**, *178*, 1071-1079.
8. Bobev, S.; Merz, J.; Lima, A.; Fritsch, V.; Thompson, J.D.; Sarrao, J.L.; Gillessen, M.; Dronskowski, R. Unusual Mn–Mn spin coupling in the polar intermetallic compounds $CaMn_2Sb_2$ and $SrMn_2Sb_2$. *Inorg. Chem*. **2006**, *45*, 4047-4054.
9. Xia, S.-Q.; Bobev, S. Diverse polyanions based on $MnBi_4$ and $MnSb_4$ tetrahedra: polymorphism, structure, and bonding in $Ca_{21}Mn_4Bi_{18}$ and $Ca_{21}Mn_4Sb_{18}$. *Inorg. Chem.* **2007**, *46*, 874-883.
10. Xia, S.-Q.; Bobev, S. Interplay between size and electronic effects in determining the homogeneity range of the $A_9Zn_{4+x}Pn_9$ and $A_9Cd_{4+x}Pn_9$ phases ($0 \leq x \leq 0.5$), *A* = Ca, Sr, Yb, Eu; *Pn* = Sb, Bi. *J. Am. Chem. Soc*. **2007**, *129*, 10011-10018.
11. Xia, S.-Q.; Hullmann, J.; Bobev, S.; Ozbay, A.; Nowak, E.R.; Fritsch, V. Synthesis, crystal structures, magnetic and electric transport properties of $Eu_{11}InSb_9$ and $Yb_{11}InSb_9$. *J. Solid State Chem*. **2007**, *180*, 2088-2094.
12. Saparov, B.; Xia, S.-Q.; Bobev, S. Synthesis, structure, and bonding of the Zintl phase $Ba_3Cd_2Sb_4$. *Inorg. Chem*. **2008**, *47*, 11237-11244.
13. Xia, S.-Q.; Bobev, S. Zintl phase variations through cation selection. Synthesis and structure of $A_{21}Cd_4Pn_{18}$ (*A* = Eu, Sr, Ba; *Pn* = Sb, Bi). *Inorg. Chem*. **2008**, *47*, 1919-1921.
14. Xia, S.-Q.; Bobev, S. Are $Ba_{11}Cd_6Sb_{12}$ and $Sr_{11}Cd_6Sb_{12}$ Zintl phases or pot? A density-functional theory study. *J. Comput. Chem*. **2008**, *29*, 2125-2133.
15. Saparov, B.; Bobev, S.; Ozbay, A.; Nowak, E.R. Synthesis, structure and physical properties of the new Zintl phases $Eu_{11}Zn_6Sb_{12}$ and $Eu_{11}Cd_6Sb_{12}$. *J. Solid State Chem*. **2008**, *181*, 2690-2696.
16. Saparov, B.; He, H.; Zhang, X.-H.; Greene, R.; Bobev, S. Synthesis, crystallographic and theoretical studies of the new Zintl phases $Ba_2Cd_2Pn_3$ (*Pn* = As, Sb), and the solid solutions $(Ba_{1-x}Sr_x)_2Cd_2Sb_3$ and $Ba_2Cd_2(Sb_{1-x}As_x)_3$. *Dalton Trans*. **2010**, *39*, 1063-1070.

17. Saparov, B.; Bobev, S. Synthesis, crystal and electronic structures of the new quaternary phases $A_5Cd_2Sb_5F$ (A = Sr, Ba, Eu), and $Ba_5Cd_2Sb_5O_x$ ($0.5 < x < 0.7$). *Dalton Trans*. **2010**, *39*, 11335-11343.
18. Saparov, B.; Bobev, S. Isolated $^{1}_{\infty}[ZnPn_2]^{4-}$ chains in the Zintl phases Ba_2ZnPn_2 (Pn = As, Sb, Bi)—Synthesis, structure, and bonding. *Inorg. Chem*. **2010**, *49*, 5173-5179.
19. Saparov, B.; Bobev, S. Pentaeuropium dicadmium pentaantimonide oxide, $Eu_5Cd_2Sb_5O$. *Acta Cryst*. **2011**, *E67*, i11.
20. Saparov, B.; Saito, M.; Bobev, S. Syntheses, and crystal and electronic structures of the new Zintl phases Na_2ACdSb_2 and K_2ACdSb_2 (A = Ca, Sr, Ba, Eu, Yb): Structural relationship with Yb_2CdSb_2 and the solid solutions $Sr_{2-x}A_xCdSb_2$, $Ba_{2-x}A_xCdSb_2$ and $Eu_{2-x}Yb_xCdSb_2$. *J. Solid State Chem*. **2011**, *184*, 432-440.
21. Brechtel, E.; Cordier, G.; Schaefer, H. Neue ternaere Erdalkali-Uebergangselement-Pnictide. *J. Less-Common Metals* **1981**, *79*, 131-138.
22. Barrett, C.S.; Cucka, P.; Haefner, K. The crystal structure of Antimony at 4.2, 78 and 298 K. *Acta Cryst*. **1963**, *16*, 451-453.
23. *SMART NT*, version 5.63; Bruker Analytical X-ray Systems Inc.: Madison, WI, USA, 2003.
24. *SAINT NT*, version 6.45; Bruker Analytical X-ray Systems Inc.: Madison, WI, USA, 2003.
25. Sheldrick, G.M. *SADABS*; University of Göttingen: Göttingen, Germany, 2003.
26. Sheldrick, G.M. *SHELXTL*; University of Göttingen: Göttingen, Germany, 2001.
27. Gelato, L.M.; Parthé, E. STRUCTURE TIDY. *J. Appl. Crystallogr.* **1987**, *20*, 139-143.
28. Jepsen, O.; Andersen, O.K. *TB-LMTO-ASA Program*, version 4.7; Max-Planck-Institut Fur Festkorperforschung: Stuttgart, Germany, 1998.
29. Andersen, O.K. Linear Methods in Band Theory. *Phys. Rev. B* **1975**, *12*, 3060-3083.
30. Andersen, O.K.; Jepsen, O. Explicit, First-Principles Tight-Binding Theory. *Phys. Rev. Lett.* **1984**, *53*, 2571-2574.
31. Lambrecht, W.R.L.; Andersen, O.K. Minimal Basis-Sets in the Linear Muffin-Tin Orbital Method—Application to the Diamond-Structure Crystals C, Si, and Ge. *Phys. Rev. B: Condens. Matter* **1986**, *34*, 2439-2449.
32. Skriver, H.L. *The LMTO Method*; Springer: Berlin, Germany, 1984.
33. Jepsen, O.; Andersen, O.K. Calculated electronic structure of the sandwich d^1 metals LaI_2 and CeI_2: Application of new LMTO techniques. *Z. Phys. B* **1995**, *97*, 35-47.